Dynamic IR-Drop Prediction through a Multi-Task U-Net with Package Effect Consideration

Yu-Hsuan Chen[1], Yu-Chen Cheng[1], Yong-Fong Chang[3], Yu-Che Lee[1], Jia-Wei Lin[3], Hsun-Wei Pao[3], Peng-Wen Chen[3], Po-Yu Chen[3], Hao-Yun Chen[3], Yung-Chih Chen[2], Chun-Yao Wang[1], Shih-Chieh Chang[1]
[1]National Tsing Hua University, Taiwan
[2]National Taiwan University of Science and Technology, Taiwan
[3]Mediatek Inc, Taiwan

***Abstract*—Dynamic IR drop analysis is a critical step in the design signoff stage for verifying the power integrity of a chip. Since the analysis is extremely time-consuming, it has led to the emergence of machine learning (ML)-based methods to expedite the procedure. While previous ML approaches have demonstrated the feasibility of IR drop prediction, they often neglect package effects and do not address diverse IR criteria for memory and standard cells. Thus, this paper introduces a novel ML-based approach designed for a fast and accurate prediction of multi-type IR drop, considering package effects. We develop new package-related features to account for the package impact on IR drop. The proposed model is based on a multi-task U-net architecture that not only predicts two types of IR drops simultaneously but also increases prediction accuracy through comprehensive learning. To further enhance the model performance, we introduce the *Input Fusion Block (IFB)*, which unifies units across channels within the input feature maps, leading to improved prediction accuracy. The experimental results show the across-pattern transferability of the proposed IR drop prediction method, demonstrating an RMSE of less than 5mV and an MAE of less than 2mV on the unseen simulation patterns. Additionally, our proposed method achieves a 5X speed-up compared to the commercial tool.**

I. Introduction

In advanced process technologies, IR drop analysis is crucial in the design signoff stage to ensure the power integrity of a chip. IR drop refers to the voltage drop in the power distribution network (PDN) of an integrated circuit (IC) when current flows through the PDN. Severe IR drop on the critical path may cause timing violations, which could further lead to functional errors. Accurate analysis necessitates considering not only the on-die PDN but also package effects on the PDN. Even in cases with low package resistance and inductance, packages can significantly impact the IR drop due to the substantial accumulated current demands of cells and current variations triggered by the concurrent switching cells.

Dynamic IR drop analysis [10] is performed by simulating the switching activities of cells to estimate the IR drop across a chip. A substantial number of simulation patterns is required to cover various operation conditions. After the analysis, different IR reports are generated and applied to various cells based on their circuit behavior. For example, *Worst-avg IR drop* is the worst of average IR drop values among all timing windows, while *worst IR drop* is the worst IR drop value during the entire simulation period. A typical design comprises both memory cells and standard cells. In the signoff stage, standard cells are evaluated by *worst-avg IR drop* to ensure the cell delay meets the specified timing constraints; memory cells are evaluated by *worst IR drop* to guarantee data integrity.

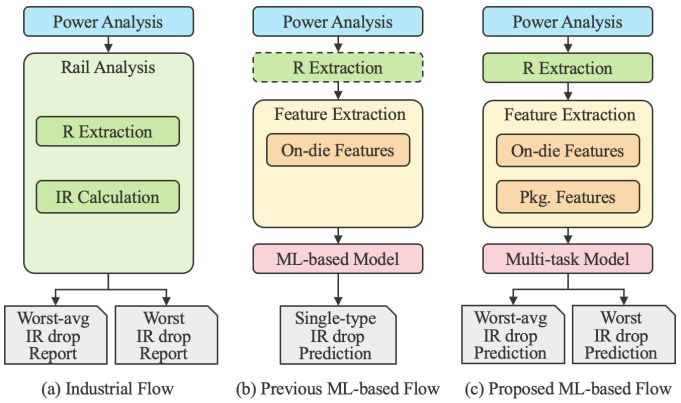

Fig. 1. Comparison of IR drop analysis flows by commercial tools and ML-based methods.

Figure 1(a) shows the industrial flow of dynamic IR drop analysis with commercial tools. Rail analysis is conducted after power analysis, and both *worst-avg IR drop* report and *worst IR drop* report are generated. Although commercial tools offer accurate IR drop analysis, the escalating number of cells in modern technology results in a prohibitively long simulation time. For example, for a design comprising around 70 million cells, a single pattern simulation in the industrial flow would exceed 40 hours. Besides, complete parallel simulation of patterns is often impractical in real-world scenarios. As a result, simulations may demand at least one week for just a few dozen patterns. Furthermore, IR signoff typically involves an iterative optimization process. Before the IR drop constraints are met, several iterations of Engineering Change Order (ECO) and dynamic IR drop analysis are performed to fix violation cells. Therefore, many machine learning (ML)-based models are explored to speed up the IR drop signoff flow.

ML-based models aim to provide a quick overview of a design's IR drop by efficiently predicting the IR drop and identifying the hotspots of a design. With quick prediction, designers can preemptively fix violation cells without waiting for IR drop reports generated by time-consuming rail analysis. Figure 1(b) shows the ML-based IR drop prediction flow of previous works [1], [3], [6]–[9], [14]. Power analysis and resistance (R) extraction are performed before model pre-

978-3-9826741-0-0/DATE25/© 2025 EDAA

diction since accurate IR drop prediction requires current-related and impedance-related information. The R extraction part is separated from rail analysis because R extraction can be performed independently by commercial tools. After feature extraction, the IR drop prediction results will be generated by the ML-based models. Notably, some studies [3], [4], [7] have employed self-defined effective distance to represent the resistance information. Although the runtime of R extraction by commercial tools can be saved, parsing additional design files to calculate effective distance incurs significant time cost. Besides, the effective distance is less accurate than resistance information obtained directly from R extraction reports.

Although prior ML-based studies have demonstrated the feasibility and efficiency of applying machine learning to IR drop prediction, there are significant challenges in integrating these methods into practical IR signoff flow for the following reasons. First, to our understanding, previous studies have not addressed the different types of IR drops. In addition, most previous studies focused on the IR drop of on-die PDN and die-related features while overlooking the package effect on IR drop issues. Therefore, prior ML-based prediction methods are unsuitable for practical IR signoff processes.

To address the aforementioned issues, we introduce a novel ML-based approach for fast and accurate multi-type IR drop prediction with the consideration of package effect. The overall flow of the proposed approach is shown in Figure 1(c). We extract and develop the on-die and package-related features to explicitly account for the package effect on IR drop. Then, we design a multi-type IR drop predictor based on the multi-task U-Net architecture. The proposed predictor not only efficiently predicts two types of IR drops simultaneously but also increases prediction accuracy through comprehensive learning. Notable enhancements in the proposed predictor include: (i) An Input Fusion Block (IFB) is designed to learn local information from both current-related and impedance-related input maps and then combine them to yield IR-related feature maps; and (ii) Channel attention layers [13] are integrated prior to the skip connections, guiding the model to focus on the most relevant feature maps for *worst-avg IR drop* and *worst IR drop* prediction separately.

The main contributions of this work are as follows:

- We propose an ML-based multi-type IR drop predictor for comprehensive learning about the *worst-avg IR drop* and the *worst IR drop*.
- We develop the new package-related features to consider the package effects on IR drop.
- We introduce the *Input Fusion Block (IFB)* for improving model performance by unifying the units of input features.
- Our proposed model with high across-pattern transferability achieves an MSE of less than 2mV and a 5X speed-up compared to the commercial tool.

The rest of this paper is organized as follows: Section II briefly reviews the related works of ML-based IR drop prediction and the background of multi-task U-Net models. Section III presents the proposed ML-based IR drop prediction approach. Section IV shows the experimental results. Finally, Section V concludes this work.

II. Preliminaries

A. IR Drop Prediction

IR drop prediction has seen the development of several ML approaches, mainly categorized into image-based [3], [6], [7], [14] and tree-based methods [1], [6]. Image-based approaches, utilizing deep learning models like Convolutional Neural Networks (CNNs) [11] and U-Net [12], convert circuit features into feature maps for model training and prediction. The model outputs can be tile-based IR drop maps or instance-based IR drop values by reverse transformation. Tree-based methods, on the other hand, employ models such as XGBoost [2], using tabular data as inputs to output instance-based IR drop values. Although tree-based approaches can directly predict instance-based IR drop values and are scalable for large feature counts, their performance is limited because the tabular data lacks spatial information about the instances in a design. Therefore, in this work, our proposed method adopts an image-based approach for enhanced IR drop prediction.

B. Multi-task U-Net Model

U-Net, derived from the traditional convolutional neural network, was first designed and applied to process biomedical images [12]. The U-Net architecture consists of an encoder and a symmetrical decoder. The encoder comprises convolutional layers that capture local features and downsampling layers that expand the receptive field of each data point. Thus, the high-dimensional features with local and global information can be extracted from the input images. The decoder employs convolutional and upsampling layers to reconstruct the target image from these high-dimensional features generated by the encoder. Moreover, the skip connection strategy is adopted to build the short paths from the encoder to the decoder. Combining low-dimensional features allows the decoder to use more precise fine-grained information for image reconstruction.

Building upon the U-Net architecture, Multi-tasking learning (MTL) model [5] extends the model's generality to handle multiple learning tasks simultaneously within a single model framework. The core principle behind MTL is to exploit commonalities and differences across tasks, leading to improved learning efficiency and prediction accuracy for these tasks. By sharing parameters and optimizing jointly for multiple tasks, MTL models demonstrate superior generalization and robustness compared to models trained on individual tasks.

Our proposed method utilizes a multi-task U-Net model to efficiently and precisely predict different types of IR drops. The detailed concepts and additional enhancements of our proposed model will be introduced in the following sections.

III. DYNAMIC IR DROP PREDICTION

In this section, we first introduce our main idea for approximate IR drop estimation, which motivates the development of both the input features and the architecture of the proposed model. Then, we show the input feature set related to on-die and package. All the input features are transformed into 2-dimensional (2D) maps for model training and prediction. Finally, we present the proposed multi-type IR drop prediction model.

A. IR Drop Estimation

Figure 2 shows the simplified equivalent die-package circuit model, which indicates that the IR drop of a cell (IR_{cell}) from the power supply to the cell's power pin comprises the IR drop contributed by the die (IR_{on-die}) and the IR drop contributed by the package (IR_{pkg}). Thus, IR_{cell} can be simply represented as:

$$\begin{aligned} IR_{cell} &= IR_{on-die} + IR_{pkg} \\ &= I_{on-die} \times Z_{on-die} + I_{pkg} \times Z_{pkg}, \end{aligned} \quad (1)$$

where I_{on-die} is the demand current of a cell, and Z_{on-die} is the equivalent impedance from a cell to the die-bump interface. I_{pkg} is the current drawn by a bump, and Z_{pkg} is the equivalent impedance of the package from a bump to the package-PCB interface.

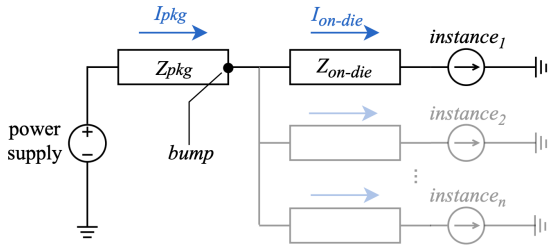

Fig. 2. Simplified equivalent die-package circuit model.

B. Feature Extraction

Based on Equation 1, we have developed four categories of input features: *on-die current-related*, *on-die impedance-related*, *package current-related* and *package impedance-related*, as shown in Table I.

1) On-die Current-related Features:

To estimate the on-die current I_{on-die} of the cells in a design, we extracted power-related features and peak current of each cell from the reports (*power.rpt*, *ptiavg files*) generated by power analysis. The power-related features represent the average current, and the peak current represents the worst-case scenarios during simulation.

- **Internal power** ($P_{i_{on-die}}$): power consumed inside the cell induced by the short current between PMOS and NMOS while the transition occurs.
- **Switching power** ($P_{s_{on-die}}$): power consumed in charging/ discharging of the output load.
- **Leakage power** ($P_{l_{on-die}}$): power consumed when the cell is idle.
- **Peak current** ($I_{peak_{on-die}}$): maximum current during the simulation period.

2) On-die Impedance-related Features:

Because the IR drop of the on-die PDN is mainly caused by the current flowing through the resistance of the on-die PDN, resistance information is necessary for IR drop prediction. Thus, we extracted effective resistance and least-resistance-path resistance to represent the resistance information from the reports generated by R extraction.

TABLE I
FEATURE LIST AND IR GROUND TRUTH.

Feature list	
On-die current-related features	Internal power ($P_{i_{on-die}}$) Switching power ($P_{s_{on-die}}$) Leakage power ($P_{l_{on-die}}$) Peak current ($I_{peak_{on-die}}$)
On-die impedance-related features	Effective resistance ($R_{eff_{on-die}}$) Least-resistance-path resistance ($R_{lrp_{on-die}}$)
Package current-related features	Bump peak current ($I_{peak_{pkg}}$)
Package impedance-related features	Effective resistance ($R_{eff_{pkg}}$) Effective inductance ($L_{eff_{pkg}}$)
IR drop label	
Standard cell	worst-avg IR drop ($IR_{worst-avg}$)
Memory cell	worst IR drop (IR_{worst})

- **Effective resistance** ($R_{eff_{on-die}}$): the effective resistance from the power pin of a cell to the die-bump interface.
- **Least-resistance-path resistance** ($R_{lrp_{on-die}}$): the resistance on the least-resistance path from the power pin of a cell to the die-bump interface.

3) Package Current-related Features:

Due to the challenges in acquiring actual measurement of bump current, we estimated the bump current in a pessimistic way. As shown in Figure 3, each on-die cell connects to every bump, and the current flowing through bumps is diverted to cells through these paths. Assuming that most of the current flows through the least-resistance path, we estimate the bump current as the sum of the peak currents from the corresponding cells along the least-resistance path. For example, in Figure 3, $bump2$ is on the least-resistance paths of cells a, b, and c. Thus, the estimated current of $bump2$ is the sum of the peak current of cells a, b, and c. Once the currents of all bumps are determined, we then utilize least-resistance paths to map these bump currents back to cells. Thus, we can obtain the estimated bump peak current feature for each cell.

- **Bump peak current** ($I_{peak_{pkg}}$): the estimated current of the bump corresponding to each cell.

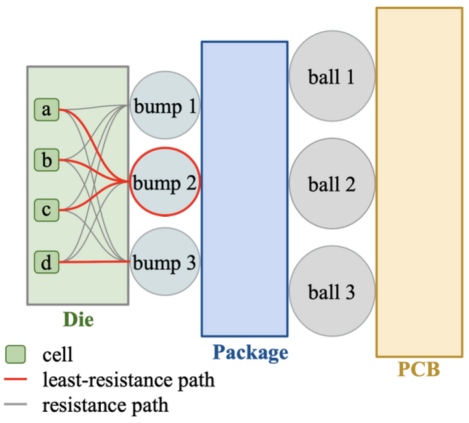

Fig. 3. Cross-sectional view of a circuit structure.

4) Package Impedance-related Features:

Because of the significant instantaneous current variation in a package, not only resistors but also inductors have a notable effect on the IR drop of a package. We extracted the effective resistance and inductance of each bump from the package reports, where the calculation of effective inductance has considered both self-inductance and mutual inductance. Then, based on the bump-cell mapping method mentioned in III-B3, we can obtain the package impedance-related features ($R_{eff_{pkg}}$, $L_{eff_{pkg}}$) of every cell.

- **Effective resistance** ($R_{eff_{pkg}}$): the effective resistance from a bump to the package-PCB interface.
- **Effective inductance** ($L_{eff_{pkg}}$): the effective inductance from a bump to the package-PCB interface.

Among the features shown in Table I, except for the power-related features, all the features have two values from power and ground pins. Therefore, there are a total of $3+(9-3)*2=15$ input features.

C. Input Feature Maps

To enable the proposed model to better account for the neighbor information of each cell in a design, we transformed the aforementioned cell-based features into 2D feature maps. Initially, cell-based features are converted into image-based features, which are composed of uniform-sized tiles. If a tile covers several cells, the value assigned to that tile is determined by the maximum feature value among these cells. Thus, the critical cells with higher IR drops are adequately represented by focusing on the maximum values.

For efficient ML-based model training and inference, these image-based features are further divided into several sub-images, termed 2D feature maps. After feature map transformation, four types of 2D feature maps ($M_{I_{on-die}}$, $M_{Z_{on-die}}$, $M_{I_{pkg}}$, and $M_{Z_{pkg}}$) and two golden IR maps ($M_{IR_{worst-avg}}$ and $M_{IR_{worst}}$) are generated for subsequent model training and prediction.

D. Multi-type IR drop Model

As shown in Figure 4, the proposed multi-type IR drop model is composed of three main components: (i) Input Fusion Block, (ii) Encoder, and (iii) Two decoders for two types of IR drop.

1) Input Fusion Block (IFB):

Drawing inspiration from the IR drop composition in Equation 1, the IFB is engineered to intake and process four distinct types of input feature maps: ($M_{I_{on-die}}$, $M_{Z_{on-die}}$, $M_{I_{pkg}}$, and $M_{Z_{pkg}}$). These maps are separately processed through convolution layers, which comprise a 3x3 depthwise convolution, a 1x1 pointwise convolution and a 3x3 convolution layer. Every convolution layer, followed by batch normalization and SiLU activation, can capture the local information of input feature maps. The output feature maps from these convolutional layers are integrated through element-wise multiplication ($\otimes$) and concatenation ($\oplus$), forging composite IR-related feature maps. Finally, these IR-related feature maps are further processed through two additional 3x3 convolution layers, producing the final input feature map for the subsequent encoder. The IFB

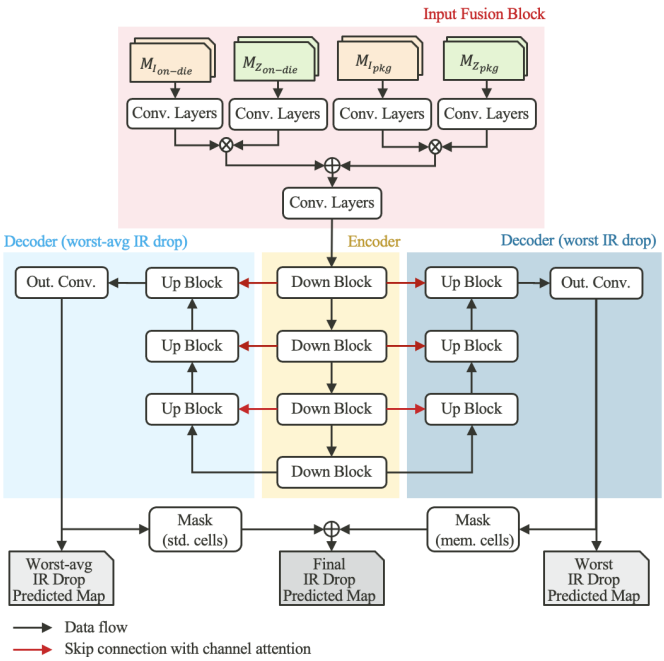

Fig. 4. Proposed multi-type IR drop model.

design ensures the consistency of feature map units of all channels to enhance the model's performance.

2) Encoder:

The encoder is designed to extract high-level information and learn the interrelations among neighboring tiles. Each *Down Block* in the encoder contains a max-pooling layer followed by two 3x3 convolution layers, which efficiently extract the high-dimensional feature maps from the low-dimensional feature maps. As feature maps are processed through a series of *Down Blocks*, the receptive field of feature maps enlarges, allowing the model to capture information from a broader neighborhood. The output feature maps of each *Down Block* are preserved for subsequent concatenation with the decoder through skip connections, facilitating the reconstruction of the output IR drop maps from the compressed representation.

3) Decoder:

In the decoder part, we employ dual decoders to separately predict two types of IR drop maps ($M_{IR_{worst-avg}}$ and $M_{IR_{worst}}$). Initially, the input feature maps of the *Up Block* are directed through an up-sampling layer followed by two 3x3 convolution layers to produce the up-sampled feature maps. For up-sampling, we utilize the pixel shuffle technique rather than traditional interpolation methods to reduce the model complexity.

The up-sampled feature maps are then concatenated with corresponding feature maps from the encoder via skip connections, enhancing the feature integration across the network. Moreover, to help two decoders focus on the most relevant feature maps for two-type IR drop prediction, we integrate the channel attention layers [13] at each skip-connection from the encoder to the decoder, as the red arrows shown in Figure 4. Lastly, the concatenated feature maps are processed through

two additional 3x3 convolution layers in the *Up Block* to generate the output feature maps of the *Up Block*.

After progressing through a series of *Up Blocks*, the worst and the worst-avg IR drop prediction maps from the two decoders are generated. Here, we define a *memory-standard-cell mask* beforehand, which is used to filter out the *memory tiles* or the *standard cell tiles* from a map. We define a tile as a *memory tile* when that tile covers no standard cells; otherwise, the tile is a *standard cell tile*. Then, we combine two IR drop prediction maps by using the *memory-standard-cell mask* to get the final IR prediction map, where the *memory tiles* are with the worst IR drop values, and the *standard cell tiles* are with the worst-avg IR drop values.

4) Loss Function:

We developed a loss function with an additional penalty term to effectively prioritize high-IR-drop regions during model training. The threshold for identifying a high-IR-drop region is set to 10% of the supply voltage. The loss function is constructed using the mean squared error (MSE) and is formulated as follows:

$$\text{loss}(\hat{y}, y) = \text{MSE}(\hat{y}, y) + [\text{MSE}(\hat{y}, y) \mid \hat{y} \geq 0.1 \cdot V_{\text{supply}}], \quad (2)$$

where $\hat{y}$ and y denote the golden and predicted IR drop values, respectively, and V_{supply} represents the supply voltage. This loss function double-weights errors in high-IR-drop regions, enhancing the model's sensitivity to critical hotspots in the design. Furthermore, we calculated the loss not only on the final IR drop prediction map, but also on the worst and worst-avg IR drop prediction maps, thereby improving the comprehensive learning of the model.

IV. Experimental Results

In this section, we demonstrate the effectiveness of our method by comparing with the vanilla U-Net [12] and three models we specifically designed to evaluate the benefits of several proposed enhancements to improve IR prediction results, including (i) the package-related feature extraction, (ii) multi-task model architecture, and (iii) *input fusion block (IFB)*. A direct comparison with previous works would be unfair, as their models are not built using our proposed feature set. We evaluate prediction results using *Root Mean Square Error (RMSE)* and *Mean Absolute Error (MAE)*. Additionally, the model's ability to identify hotspots will be evaluated using *Recall* and *Precision*.

TABLE II
Statistics of Simulation Patterns

Pattern ID	#Violation cells	Max IR drop (mV)	Avg. pkg. IR pct. (%)
1	3102	169.91	25.98
2	838	166.39	27.52
3	10976	159.89	23.19
4	14856	173.0	33.25

A. Experimental Setup

We evaluated the proposed methods on an industrial design with an area of $4974\mu m \times 4630\mu m$, comprising approximately 50 million cells. The supply voltage is 0.9V, and the process technology is TSMC's 4nm process. The input feature maps and golden IR maps consist of 496×496 tiles, with each tile sized $1\mu m \times 1\mu m$.

We used four *300ns* simulation patterns in our experiment. Detailed statistics for these patterns are provided in Table II. The number of violation cells and maximum IR drop indicate the severity of IR drop. The average package IR percentage reflects the average contribution of the package to the overall IR drop of each cell.

To effectively capture the dynamic IR drop violation, all *300ns* patterns were segmented into ten *30ns* slices. We evaluated the model by training on three patterns (30 slices) and testing on the remaining unseen pattern (10 slices). This evaluation method demonstrates the model's generalization capability and transferability across various patterns.

The proposed model was implemented using PyTorch and trained on eight NVIDIA A6000 GPUs. We used the Adam optimizer with an initial learning rate of 0.001, which was adjusted by cosine decay to optimize learning convergence. The model takes 300 minutes for one-shot training over 600 epochs.

B. Dynamic IR Drop Prediction Results

To evaluate the benefits of the proposed enhancements, we implemented four models for comparison, including:

- ***Vanilla U-Net* [12]**: the baseline model consists of a single encoder and decoder, utilizing only on-die feature maps ($M_{I_{on-die}}$, $M_{Z_{on-die}}$).
- ***+multi***: the multi-type IR drop model with two decoders to predict two types of IR drop maps (*worst-avg IR* and *worst IR*).
- ***+multi+PKG***: the model based on *+multi* architecture with the on-die-related and package-related input feature maps ($M_{I_{on-die}}$, $M_{Z_{on-die}}$, $M_{I_{pkg}}$, $M_{Z_{pkg}}$).
- ***+multi+PKG+IFB***: Our proposed model, as illustrated in Figure 4, integrates all the aforementioned enhancements.

Table III presents the models' prediction performance and hotspot identification abilities. For prediction performance, our proposed model achieves the lowest *RMSE* and *MSE* across all unseen test patterns compared to the other three models. Furthermore, we observe that each proposed enhancement

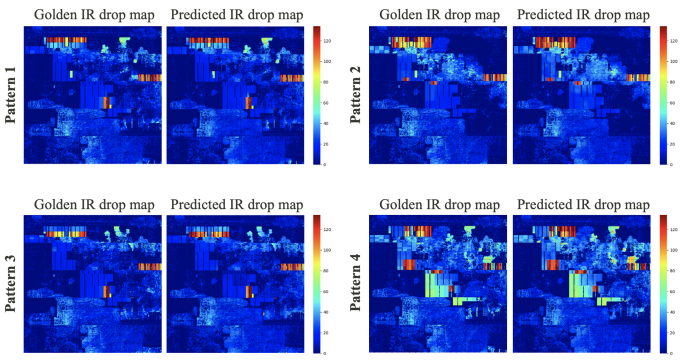

Fig. 5. Golden IR drop maps vs. Predicted IR drop maps of the proposed model.

TABLE III
IR DROP PREDICTION PERFORMANCE.

Prediction results								
Model	Pattern 1		Pattern 2		Pattern 3		Pattern 4	
	RMSE	MAE	RMSE	MAE	RMSE	MAE	RMSE	MAE
Vanilla U-Net [12]	3.57	1.85	3.44	1.88	5.34	1.96	5.13	2.00
+multi	3.43	1.74	3.67	1.99	4.62	1.63	4.68	1.76
+multi +PKG	3.3	1.71	3.39	1.79	4.52	1.54	4.65	1.70
+multi +PKG +IFB	**3.11**	**1.61**	**3.2**	**1.71**	**4.0**	**1.34**	**4.50**	**1.64**
Hotspot identification results								
	Recall	Precision	Recall	Precision	Recall	Precision	Recall	Precision
Vanilla U-Net [12]	0.89	**0.83**	0.90	**0.85**	0.70	**0.91**	0.73	**0.95**
+multi	0.94	**0.83**	0.94	0.73	0.85	0.83	0.86	0.87
+multi +PKG	0.94	0.81	0.93	0.69	0.86	0.81	0.87	0.87
+multi +PKG +IFB	**0.96**	0.77	**0.96**	0.69	**0.90**	0.81	**0.91**	0.84

progressively reduces *RMSE* and *MSE*, indicating that these enhancements are effective for improving IR drop prediction.

For the hotspot identification, we set the 10% of the supply voltage as the threshold for determining the hotspot tiles. *Recall* means the percentage of actual hotspot tiles captured by the model; *Precision* means the percentage of actual hotspot tiles among the hotspot tiles predicted by the model. We aim to identify a design's hotspots to allow designers to preemptively fix violation regions. Consequently, we pay more attention to Recall than Precision. According to Table III, we can observe that *Vallina U-Net* has weaker hotspot identification ability on *Pattern 3* and *Pattern 4*, which have a large number of violation instances. However, our proposed model can capture over 90% violation tiles for unseen testing patterns. In Figure 5, we show the prediction and golden heatmaps of a slice from four patterns. Compared to golden IR drop maps, our prediction maps successfully capture most of the real hotspots, which is reflected our model's excellent performance in terms of *Recall*.

TABLE IV
RUNTIME COMPARISON BETWEEN INDUSTRIAL FLOW AND PROPOSED ML-BASED FLOW.

Industrial flow		Proposed ML-based flow	
Stage	Runtime	Stage	Runtime
Power analysis	14 hrs	Power analysis	3 hrs
Rail analysis	25 hrs	R extraction	3 hrs
		Feature extraction	1 hrs
		IR prediction	3 mins
Total	39 hrs	Total	7 hrs

C. Runtime

Table IV shows a detailed runtime comparison of the industrial flow with a single *300ns* simulation pattern and our proposed flow with ten *30ns* simulation slices. Analyzing a single *300ns* simulation pattern by the commercial tool typically requires about 40 hours in the industrial flow, where the power analysis takes about 14 hours, and the rail analysis takes about 25 hours. In our proposed flow, power analysis and R extraction are necessary for extracting current and resistance information for our model. We compare the runtime of R extraction, feature extraction, and IR drop prediction in our proposed flow against the rail analysis in the industrial flow. As shown in Table IV, our proposed IR drop prediction method can achieve a 5X speed-up compared to the industrial flow.

D. Discussion for Model Prediction Error

While the prediction results demonstrate the effectiveness of our method, some prediction errors are inevitable. We have identified two main causes for these errors.

First, our model evaluates standard cells using the worst-average IR drop, but the input features lack specific timing window information. To streamline feature extraction and processing, we use power and peak current features to represent average and worst-case current scenarios. This approach avoids the complexities and significant preprocessing time required to parse detailed timing window information.

Second, there is a timing discrepancy between the current-related features and the IR drop values. To stabilize cell signals in a design, a pre-simulation period is required for accurate IR drop analysis. In our experiments, we set a $35ns$ pre-simulation time for each $30ns$ slice. Thus, the tool reports the current-related information over a total $65ns$ simulation time, but only reports IR drop information of the targeted $30ns$ simulation window. This discrepancy is due to the inherent limitations of the used commercial tool, leading to unavoidable differences between the input features and the IR drop labels.

Despite these prediction errors, the IR drop prediction from our proposed method still exhibit a strong correlation with the golden IR drop values. Thus, our method provides a low prediction error and a high-recall IR drop quick-view, significantly accelerating the IR signoff stage.

V. CONCLUSION

We have proposed a multi-type IR drop model for a fast and accurate dynamic IR drop prediction. Our method makes three main contributions: (i) the package-related input features development, (ii) multi-type IR drop prediction, and (iii) the *Input Fusion Block (IFB)* for unifying the units of the input feature maps. Our experimental results demonstrate the across-pattern transferability of our proposed model with an RMSE of less than *5mV* and an MSE of less than *2mV* on the unseen simulation patterns. Moreover, our proposed model can identify over 90% hotspots in the design while achieving a 5X speed-up compared to the industrial IR drop analysis using *Voltus*.

REFERENCES

[1] Jia-Xian Chen et al. Vector-based dynamic IR-drop prediction using machine learning. In *Asia and South Pacific Design Automation Conference*, pages 202–207, 2022.

[2] Tianqi Chen and Carlos Guestrin. XGBoost: A scalable tree boosting system. In *ACM SIGKDD Conference on Knowledge Discovery and Data Mining*, pages 785–794, 2016.

[3] Vidya A Chhabria et al. MAVIREC: ML-aided vectored IR-drop estimation and classification. In *Design, Automation & Test in Europe Conference & Exhibition*, pages 1825–1828, 2021.

[4] Vidya A Chhabria et al. Thermal and IR drop analysis using convolutional encoder-decoder networks. In *Asia and South Pacific Design Automation Conference*, pages 690–696, 2021.

[5] Michael Crawshaw. Multi-task learning with deep neural networks: A survey, 2020.

[6] Yen-Chun Fang et al. Machine-learning-based dynamic IR drop prediction for eco. In *International Conference on Computer-Aided Design*, pages 1–7, 2018.

[7] Yonghwi Kwon et al. Dynamic IR drop prediction using image-to-image translation neural network. In *International Symposium on Circuits and Systems*, pages 1–5, 2021.

[8] Shih-Yao Lin et al. IR drop prediction of ECO-revised circuits using machine learning. In *VLSI Test Symposium*, pages 1–6, 2018.

[9] Seyed Nima Mozaffari et al. An efficient supervised learning method to predict power supply noise during at-speed test. In *International Test Conference*, pages 1–10, 2019.

[10] SK Nithin et al. Dynamic voltage (IR) drop analysis and design closure: Issues and challenges. In *International Symposium on Quality Electronic Design*, pages 611–617, 2010.

[11] Keiron O'Shea and Ryan Nash. An introduction to convolutional neural networks. *CoRR*, abs/1511.08458, 2015.

[12] Olaf Ronneberger et al. Convolutional networks for biomedical image segmentation. In *Asia and South Pacific Design Automation Conference*, page 234–241, 2015.

[13] Sanghyun Woo et al. Cbam: Convolutional block attention module. In *European conference on computer vision*, pages pp.3–19, 2018.

[14] Zhiyao Xie et al. PowerNet: Transferable dynamic IR drop estimation via maximum convolutional neural network. In *Asia and South Pacific Design Automation Conference*, pages 13–18, 2020.